OPTOELECTRONİCS AND ADVANCED MATERİALS – RAPİD COMMUNİCATİONS Vol. 1, No. 3, March 2007, p. 100 - 107

Electronic structure and optical properties of $KNbO_3$: First principles study

SULEYMAN CABUK
Cukurova University, Faculty of Science and Letters, Physics Department, Adana, 01330, Turkey

The electronic structures and optical properties of $KNbO_3$ were studied from the first principles using density functional theory. The energy band structures, dielectric function and optical constants of cubic and tetragonal phases are calculated using pseudopotential with local density approximation. A direct band gap at Γ point and an indirect band gap R- Γ point in the Brillouin zone are predicted for cubic and tetragonal phases. Both phases, the real and imaginary parts of the dielectric function and hence the optical constants such as reflectivity, refractive index, extinction coefficient, electron energy-loss function, ε_{eff} (the optical dielectric constant) and N_{eff} (the effective number of electrons) per unit cell are calculated. The calculated spectra are compared with the experimental data in the orthorhombic phase and other theoretical results for $KNbO_3$ and are found to be in good agreement with the results.

(Received December 19, 2006; accepted February 14, 2007)

Keywords: Electronic structure, Optical properties, Perovskite structure, $KNbO_3$

1. Introduction

Ferroelectric and related perovskites having chemical formula ABO_3 are interesting from their technical importance and the physics of their phase transitions [1]. Within this family of materials, one finds transitions to a wide variety of low-symmetry phases, including ferroelectric and antiferroelectric transitions. The ideal structure is cubic perovskite, where the A and B cations are arranged on a simple cubic lattice and the O ions lie on the face centers nearest the B cations. The B cations sits at the center of each oxygen octahedra while the A cations lie at the larger 12-fold coordinated sites between the octahedra. Their simple structures allow extensive theoretical investigation. The ferroelectric transition occurs as a result of a delicate balance between long-range Coulomb interactions and short-range forces. Thus this ideal structure displays a wide variety of structural instabilities in the various materials. These may involve rotations and distortions of the O octahedral as well as displacements of the cations from their ideal sites. The interplay of these instabilities accounts for the rich variety of ferroelectric and antiferroelectric behaviors. The dielectric and optical properties of the perovskites are very important. The energy gap lies in the visible region of the spectrum and this is one reason why these materials are interesting [2-5]. Thus, the optical properties of the perovskites are anisotropic and they are known to show the phenomenon of birefringence. The optical and dielectric properties of many of the perovskites have been measured extensively and accurately [6]. However, the theoretical treatment of the optical properties is lagging behind the measurements. This is partly due to the fact that when the measurements were made, a microscopic theoretical understanding was not available. With the advancement of the theoretical method to treat the electronic structure in combination with the development of fast computers, there are several first-principles methods available for calculation of optical, electronical, structural and dynamical properties of the perovskite.

Potassium niobate ($KNbO_3$) is one of the most studied members in the important class of perovskite structure ferroelectrics. Extensive theoretical and experimental studies have been carried out since the discovery of the ferroelectricity in this compound [7]. Due to its technological importance, $KNbO_3$ has been subject to numerous ab initio electronic structure calculation. Like $BaTiO_3$, $KNbO_3$ undergoes three successive ferroelectric phase transitions, from cubic to tetragonal at 691 K, tetragonal to orthorhombic at 498 K, and orthorhombic to rhombohedral at 263 K. $KNbO_3$ has tetragonal symmetry between 498 and 691 K and is ferroelectric, which belongs to the P4mm-C_{4v}^1 symmetry group. At 691 K it undergoes a transition to cubic and paraelectric state having space group Pm3m-O_h^1 [8]. Many of the calculation were based on the local density approximation (LDA) [9] combined either [10,11] with the linearized muffin-tin orbital (LMTO)[12] or with the pseudopotential method [13,14] as well as with the linearized augmented plane wave (LAPW) [15-17] scheme. Several ab initio self-consistent energy band structure calculations have been reported for $KNbO_3$ [18-20]. Most of them were aimed at the description of the ground-state properties. We present here a detail calculation of the optical properties $KNbO_3$ using one of the current state-of-the-art methods, namely, the pseudopotential method based on density functional theory in the local density approximation. The optical properties of ground state orthorhombic phase of $KNbO_3$ have been studied experimentally [21]. Theoretical studies [22-25]

have been performed on both the orthorhombic and cubic phases of $KNbO_3$. In this work, we have made first principles pseudopotential calculations of the electronic band structure and optical properties of $KNbO_3$ in both the cubic and tetragonal phases. We have also made some comparisons with related experimental and theoretical data where available.

2. Computational procedures

All calculations were carried out within the local density approximation (LDA) of density functional method for cubic and tetragonal phase $KNbO_3$. The self-consistent norm-conserving pseudopotentials are generated using the Troullier-Martins scheme [26] which is included in the FHI98PP package [27]. Plane waves are used as a basis set for the electronic wave functions (in the perovskite structure there are five atoms per unit cell, and this structure is a very open structure; packing fraction=0.32). In order to solve the Kohn-Sham equations [28], the conjugate gradient minimization method [29] is employed as implemented by the ABINIT code [30-31]. The exchange correlation effects are taken into account within the Perdew-Wang scheme [32] as parameterized by Ceperly and Alder [33]. The DOS has been calculated by the method of tetrahedra [34]. The calculations have been performed considering the origin of the cell to be at K site, Nb at the body-centre (0.5, 0.5, 0.5)a and the three O atoms at the three face centers (0.5, 0.5, 0.0)a, (0.5, 0.0, 0.5)a, and (0.0, 0.5, 0.5)a. The calculation were carried out using experimental data for lattice constants a = b = c = 4.0214 Å in the cubic phase. For the tetragonal structure, we used the crystallographic data with lattice constant of a = b = 3.997 Å and c = 4.063 Å [7]. The experimental ferroelectric structure is obtained from that by displacing the ions off center, by u. The experimental values [35] in units of c and keeping the origin fixed at Nb, are u_K = -0.023, u_{OI} =-0.040, and u_{OII} =-0.042, where the subscript O_I refers to top and bottom oxygen ions in the basal plane of the octahedron. Pseudopotentials are generated using the following electronic configurations: For K $4s^1$ electron is considered as the true valence. For O only the true valence states ($2s^2$ and $2p^{4)}$ are taken into account. For Nb $4d^4$ $5s^1$ the electron states are treated as valence states. The above configuration is found to be the optimized choice for these materials.

The optical properties may be extracted from the knowledge of the complex dielectric function, $\varepsilon(\omega) = \varepsilon_1(\omega) + i\,\varepsilon_2(\omega)$. The imaginary part, $\varepsilon_2(\omega)$, was calculated from the momentum matrix elements between the occupied and unoccupied wave functions. The real part $\varepsilon_1(\omega)$ of dielectric function $\varepsilon(\omega)$ follows from the Kramers-Kronig relationship. In the tetragonal phase, $\varepsilon(\omega)$ is anisotropic and has two different components, $\varepsilon_{xx}(\omega)$ and $\varepsilon_{zz}(\omega)$, corresponding to the electric field perpendicular and parallel to c-axis, respectively. In our case, the plane-wave kinetic energy cutoff has been raised to 35 eV, and using 8 × 8 × 8 the Monkhorts-Pack [36] k-point mesh grid. We have found that in the band structure calculations 40 k points are enough to obtain good results for this transition-metal oxides. In the calculations of the density of states, however, the irreducible Brillouin zone was sampled with 512 k points for $KNbO_3$.

3. Results and discussion

3.1. Structural parameters

The theoretical lattice constants were obtained for the cubic by minimizing the ratio of the total energy of the crystal to its volume. In Table 1, we compare the present result for the lattice parameter of cubic $KNbO_3$ with previous theoretical and experimental values. This is within the accuracy range of calculations based on density functional LDA. In the case of cubic $KNbO_3$, comparisons of our results with the first principles work and with the calculated values suggest that our pseudopotentials are reliable and work slightly better.

Table 1. Comparision of present result for lattice parameters of cubic $KNbO_3$ with previous theoretical and experimental values.

	Lattice parameter (Å)	Error (%)
(LDA) PW-CA(this work)	a = 3.950	-1.77
(LDA) USP [37]	a = 3.951	-1.75
(LDA) LAPW+LO [39]	a = 3.960	-1.52
(GGA) PBE[38]	a = 4.009	-0.31
(GGA) FP-LMTO[25]	a = 4.039	0.44
LMTO-ASA[18]	a = 3.940	-2.02
LAPW+LO(WDA)[39]	a = 4.011	-0.26
FP-LMTO[10]	a = 3. 930	-2.28
Exp. value at 698 K[7]	a = 4.0214	-
(Extrapolated value at 0K)[39]	(a = 4.016)	-

PW-CA: Perdew-Wang scheme as parameterized by Ceperly and Alder, USP: ultrasoft pseudopotentials, GGA: the generalized gradient approximation, PBE: Perdew Burke Ernzahof, LAPW+LO: linearized augmented plane-wave method with local orbital extensions, WDA: weight density approximation, LMTO-ASA: atomic sphere approximation of linearized muffin tin orbital method. FP-LAPW: full-potential linearized augmented plane wave,

We calculated the relaxed crystal structure of tetragonal $KNbO_3$. The lattice parameters, a and c, were optimized by the minimization of the total energy. The lattice parameters of $KNbO_3$ in the tetragonal structure obtained using various exchange-correlation function are summarized in Table 2. We compare the present results for the lattice parameters of tetragonal $KNbO_3$ with the first principles work and the calculated values. It is found to be in good agreement with the calculations.

Table 2. Comparision of present results for lattice parameters of tetragonal $KNbO_3$ with previous theoretical and experimental values.

	Lattice parameter (Å)	Error (%)
(LDA) (this work)	a = 3.950	-1.17
	c = 3.983	-1.96
(LDA) CA-PZ[33]	a = 3.939	-1.45
	c = 3.983	-1.96
(GGA) PBE[38]	a = 3.984	-0.32
	c = 4.146	2.04
(GGA) RPBE[45]	a = 3.932	-1.62
	c = 4.763	17.22
(GGA) PW91[32]	a = 3.983	-0.35
	c = 4.134	1.74
Experimental value[7]	a = 3.997	-
	c = 4.063	-

3.2. Band structure

The band structures and densities of states of $KNbO_3$ is plotted along high symmetry axes of the Brillouin zone for the cubic (Fig. 1) and tetragonal phase (Fig. 2). The energy scale is in eV and the origin of energy was arbitrarily set to be at the valence band maximum. High-symmetry points in the Brillouin zone include: Γ (0,0,0); X(1/2,0,0); M(1/2,1/2,0); and R(1/2,1/2,1/2). The electronic structure of valence bands, the band gap, and low-energy conduction bands determine the most important properties of the material in electronic device application. In cubic structure, the bottom band between about -16 eV and -17 eV originates from O (2s) orbital. Nine valence bands near Fermi level between 0.0 and -5 eV are derived from O(2p) orbital. The valence band complex ranging from 0.0 to -5 eV is formed by p-orbitals of O(2p). The valence bands are separated from the conduction bands by a direct band gap of 2.395 eV at the symmetry point (Γ). It is clear that the band gap appears between the top-most valence band at R-point and the bottom-most conduction band at Γ-point. Our calculated value of the indirect band gap of $KNbO_3$ is 1.460 eV. These calculated values are smaller than the experimental value of 3.3 eV [40]. The electronic structure of tetragonal structure in Fig. 2 is very similar to that of cubic structure, as may be expected. For tetragonal $KNbO_3$ the calculated indirect energy-band gap is found to be 1.504 eV and the direct band gap is 2.572 eV. Table 3 collects the values of the energy gap of $KNbO_3$ with previous theoretical and experimental values. The optical band gap in both phases change by about 0.178 eV (direct band gap) and 0.040 eV (indirect band gap). The origin of these discrepancy may be the local density approximation which underestimates the band gaps even for insulators. There are some experimental complications in determining the exact band gap, including the optical absorption edge tails which extend to several tenths [1]. In cubic phase, the nine valence bands at Γ point are the three triply degenerate levels (Γ_{15}, Γ_{25} and Γ_{15}) separated by energies of 1.695 eV (Γ_{15}- Γ_{25}) and 0.231 eV (Γ_{25}- Γ_{15}). These splittings are produced by the crystal field and the electrostatic interaction between O (2p) orbitals. In the conduction band the triply (($\Gamma_{25'}$) and doubly (Γ_{12}) degenerate levels represent t_{2g} and e_g states of Nb 4d orbitals separated by an energy of 3.847 eV. In the tetragonal phase, the nine valence bands are split into a triply (Γ_{15} = -2.844 eV), three doubly (-1.615, -1.214 and -0.982 eV) degenerate levels at the Γ point. In the conduction band, the two doubly ($\Gamma_{25'}$ and Γ_{12}) degenerate levels represent Nb 4d orbitals separated by an energy of 3.434 eV. This change in electronic band structure of $KNbO_3$ with change of symmetry is also related to the availability of spontaneous polarization in the tetragonal phases. To further elucidate the nature of electronic band structure, we have also calculated the total densities of state of cubic (Fig. 1) and tetragonal (Fig. 2) $KNbO_3$. The DOS for tetragonal and cubic phases of $KNbO_3$ are quite similar, showing that the effect of tetragonality on band structure is very small, in agreement with Michael-Calendini and Meslard results [42].

Table 3. Comparison of theoretical and experimental band gap (in eV) of $KNbO_3$ structure.

	Cubic	Tetragonal
Band gap Γ-Γ (this work)	2.395	2.572
(direct)	2.20[23]	
	2.23[25]	
Band gap Γ-R (this work)	1.460	1.504
(indirect)	1.40[18]	
	1.58[25]	
	1.43[22]	
Experimental	3.30[40]	4.42 [41]

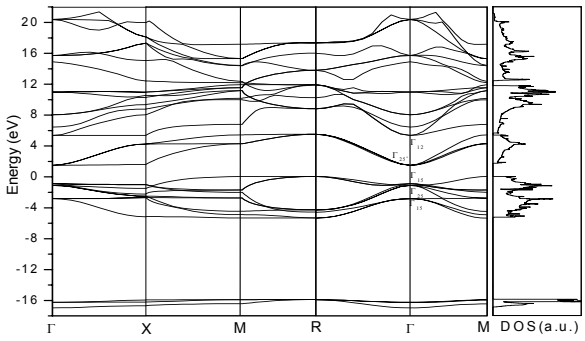

Fig. 1. Band structure along the high symmetry directions in the Brillouin zone and total density of state in cubic phase.

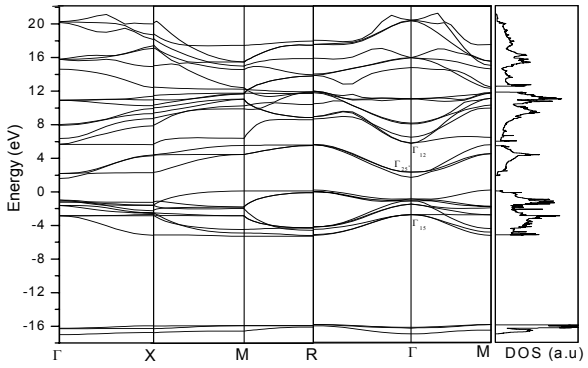

Fig. 2. Band structure along the high symmetry directions in the Brillouin zone and total density of state in tetragonal phase.

3.3. Dielectric function

We calculated the optical properties of $KNbO_3$ in the cubic and tetragonal phase. In cubic phase, the real and imaginary parts of dielectric function are shown in Fig. 3 and 4 for $KNbO_3$. The values of two main peaks of $\varepsilon_1(\omega)$ curve are 3.23 and 2.94 at energy equal 7.58 and 8.66 eV, respectively, and for $\varepsilon_2(\omega)$ are 2.13 and 2.99 at energy equal 8.10 and 8.87 eV, respectively. In Fig. 3 and 4 we have compared our calculated $\varepsilon_1(\omega)$ and $\varepsilon_2(\omega)$ spectra with experimental data [21] for $KNbO_3$ in the orthorhombic phase. There is observed that the theoretical peak at 7.58, 8.66 eV for $\varepsilon_1(\omega)$ and 8.10, 8.87 eV for $\varepsilon_2(\omega)$ are lower in amplitude than the experimental values (4.96, 8.34 eV for $\varepsilon_1(\omega)$ and 5.08, 9.09 eV for $\varepsilon_2(\omega)$). These facts could be interpreted as being probably due to the neglect of excitonic and local field effects. Fig. 5 and 6 show the real and imaginary parts of dielectric functions for $KNbO_3$ in the tetragonal phase along the a and c crystallographic axes. Symbols C, T_xx and T_zz refer to cubic, tetragonal crystallographic axis and tetragonal c axis, respectively. The general behavior of $\varepsilon_1(\omega)$ for tetragonal phase curve is similar to that for cubic phase. The main peak of $\varepsilon_2(\omega)$ for tetragonal phase curve has a peak in the range of 9.05 eV (a crystallographic axis) and 9.99 eV (c crystallographic axis). If we assume an orientation of the crystal surface parallel to the optical axis, the reflectivity of the crystal $R(\omega)$ derived from Fresnel's formula is:

$$R(\omega) = \left(\frac{\sqrt{\varepsilon(\omega)} - 1}{\sqrt{\varepsilon(\omega)} + 1} \right)^2 \quad (1)$$

In the case of interband transitions, which consist mostly of plasmon excitations, the scattering probability of volume losses is directly related to the energy loss function [43].

$$-\mathrm{Im}(1/\varepsilon) = \frac{\varepsilon_2}{\varepsilon_1^2 + \varepsilon_2^2} \quad (2)$$

Also, the optical functions such as the refractive index, $n(\omega)$, and the extinction coefficient, $k(\omega)$, are calculated in terms of the components of the complex dielectric function as follows:

$$n(\omega) = (1/\sqrt{2})\left[\varepsilon_1(\omega) + \sqrt{\varepsilon_1(\omega)^2 + \varepsilon_2(\omega)^2}\right]^{1/2} \quad (3)$$

$$k(\omega) = (1/\sqrt{2})\left[\sqrt{\varepsilon_1(\omega)^2 + \varepsilon_2(\omega)^2} - \varepsilon_1(\omega)\right]^{1/2} \quad (4)$$

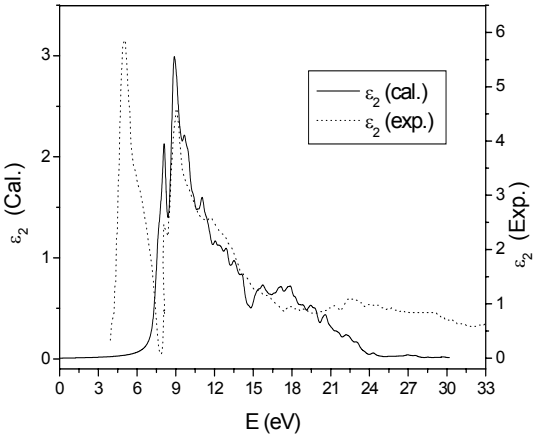

Fig. 3. Imaginary part of the dielectric function for $KNbO_3$ in cubic and orthorhombic phase.

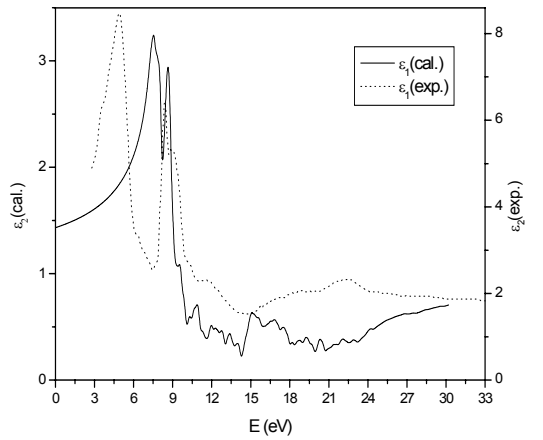

Fig. 4. Real part of the dielectric function for $KNbO_3$ in cubic and orthorhombic phase.

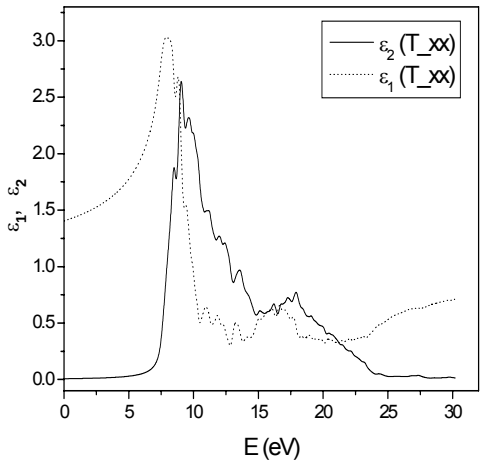

Fig. 5. Real and imaginary part of the dielectric function for $KNbO_3$ in tetragonal phase along the a crystallographic axe.

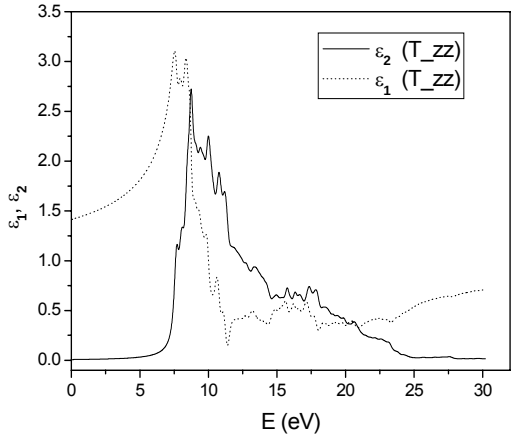

Fig. 6. Real and imaginary part of the dielectric function for $KNbO_3$ in tetragonal phase along the c crystallographic axe.

We calculated the spectral reflectivity, the refractive index, extinction coefficient and electron energy loss function with a simple independent program. The energy loss function is plotted for cubic and tetragonal phase in Fig. 7. These peaks can have different origins such as binding electron oscillations (plasmon) and interband or intraband excitations. In cubic phase, the energy of the maximum peak of Im($-\varepsilon^{-1}$) at 22.46 eV is assigned to the energy of volume plasmon. The first peak at 13.16 eV originates from O-2p to Nb 4d and second peak is at 20.79 eV (surface plasmon). In tetragonal phase, the energy of the maximum of Im($-\varepsilon^{-1}$) is smaller than cubic phase and equal 22.23 eV (a-direction) and 20.94 (c-direction). The reflectivity spectra are shown in Fig. 8. The calculated reflectivity are shown with curves, while crosses show the measured results [21]. The spectra exhibit peaks similar to those in the dielectric function. We find also that the reflectivity varies widely as a function of energy. This could possibly make the compound $KNbO_3$ suitable for a variety of optical applications. It is important to note that the discrepancy between the theoretically calculated reflectivity spectra and the experimental results [21] is perhaps due to the fact that the measured reflectivity is for orthorhombic $KNbO_3$. The deviations may therefore reflect the strong charges in the Nb 4d derived conduction band produced by the displacements of atoms from their positions in the perovskite structure. The calculated refractive index and extinction coefficient of cubic and tetragonal phases are presented in Fig. 9, 10. As can be seen from Fig. 9, 10 the normal dispersion is in the 0-9 eV energy range. This is consistent with the results for $\varepsilon_2(\omega)$ shown in Fig. 3. The photon energy range between 9 eV and 24 eV corresponds to an absorption region.

3.4. Sum rules and effective number of valence electrons

Another way to consider the number of electrons involved in the valence interband transition is to evaluate the sum rule [44]. The effective number of valence electron N_{eff} and the optical dielectric constant ε_{eff}, which make contribution to the optical functions of a crystal at the energy E_0, contribute per unit cell to a transition up to frequency ω can be calculated using the sum rule

$$N_{eff} = \frac{2m\varepsilon_0}{\pi\hbar^2 e^2}\frac{1}{N_a}\int_0^{E_0}\varepsilon_2(E')E'dE' \qquad (5)$$

$$\varepsilon_{eff} = 1 + \frac{2}{\pi}\int_0^{E_0}\varepsilon_2(E')E'^{-1}\,dE' \qquad (6)$$

where N_a is the density of atoms in a crystal. The physical meaning of ε_{eff} is quite clear: ε_{eff} is the effective optical dielectric function governed by interband transition in the energy range from zero to E_0, i.e., by the polarization of the electron shell. The calculated effective optical dielectric constant for $KNbO_3$ is shown in Fig. 11. N_{eff} of cubic and tetragonal structure are very similar to each others. Both phases, N_{eff} rise rapidly between 8 eV and 12 eV, and then there are another rise, and finally, saturation at a value near 25 eV. The experimental data rose almost monotonically on increase in the photon energy and show no tendency to saturation throughout the investigation energy range. Therefore, it is possible to select some independent criteria for estimating the number of valence electrons per unit cell. Our values

of N_{eff} (calculated using the nominal ion charges) are of the same order of magnitude at these energies as the other calculated values. The photon energy dependence of the ε_{eff} obtained by us for $KNbO_3$ is curve (Fig. 12) which can be separated into two regions both phases. The first is characterized by a rapid rise between 7.5 eV and 11 eV [experimental ~ 5 - 12 eV]. In the second region the ε_{eff} rises more smoothly and slowly to saturation at energies 25 eV [exp. ~30 eV]. This mean that the greatest contribution to ε_{eff} is made by the transitions corresponding to the bands between 7.5 and 11 eV (their contribution amount to 80 %) [exp. ~ 5 eV and ~10 eV, 85%, respectively].

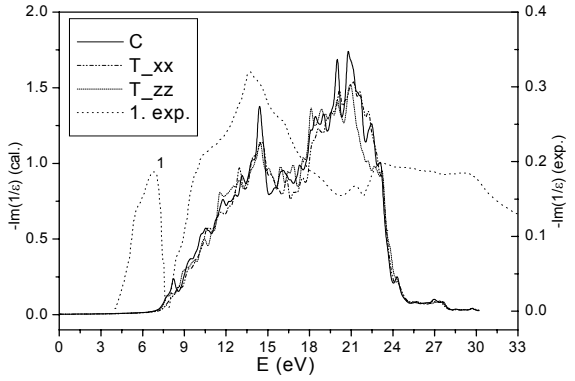

Fig. 7. Energy loss function versus photon energy for $KNbO_3$.

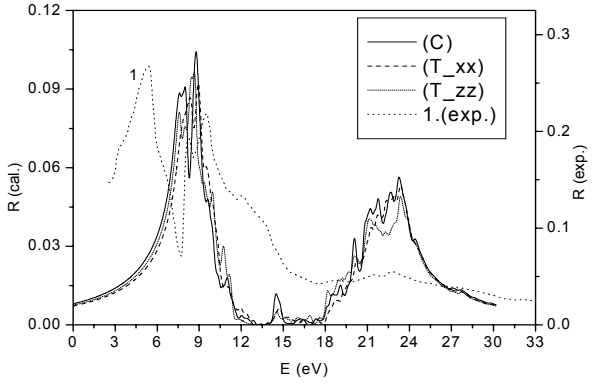

Fig. 8. The reflectivity spectra for $KNbO_3$.

The contribution made to static dielectric function $\varepsilon(0)$ by optical transition at photon energies $E > E_0$ makes ε_{eff} to vary with the square of the refractive index n^2 measured (or calculated) in the transparency range. The difference $\delta\varepsilon = n^2 - \varepsilon_{eff} \neq 0$ (n_{cubic}≈2.35 [46], ε_{eff} =2.4, $\delta\varepsilon = 3.12$) shows the need to allow for the polarizability of deep-lying levels (semicore and core bands).

Generally, we have performed the calculations over a wide energy range leading to very high energy transitions such that contributions originating from each of the atoms will be accommodated. It is to be noted that there are no experimental results for the optical properties for the cubic and tetragonal phase $KNbO_3$. We expect that our theoretical studies will motivate experimental work aimed to investigate the optical properties of cubic and tetragonal structure of this compound.

4. Conclusions

We calculated the electronic and optical properties of $KNbO_3$ in both cubic and tetragonal phases using an *ab initio* pseudopotential method with LDA. The DOS and band structure for tetragonal and cubic phases of $KNbO_3$ are quite similar, showing that the effect of tetragonality on band structure is very small. The cubic and tetragonal structures of $KNbO_3$ are predicated to be indirect gap materials. Our results for electronic properties of both phases are shown to agree with other calculations and experimental findings. It is found that there is significant hybridization between Nb d and O p states in the compound. We have studied the optical properties such as the dielectric function, reflectivity, electron energy-loss function, ε_{eff} and N_{eff} and compared with the experimental results at room temperature for $KNbO_3$ in the orthorhombic phase. The optical constants for the two phases have noticeable small differences, suggesting that tetragonality leads to a significant change in the wave functions affecting the height and position of the peaks in the optical spectra. Using the band structure, we have analyzed the interband contribution to the optical response functions. It is found that the origin of the peaks in the dielectric function probably also explains the structures in the spectra of these optical functions.

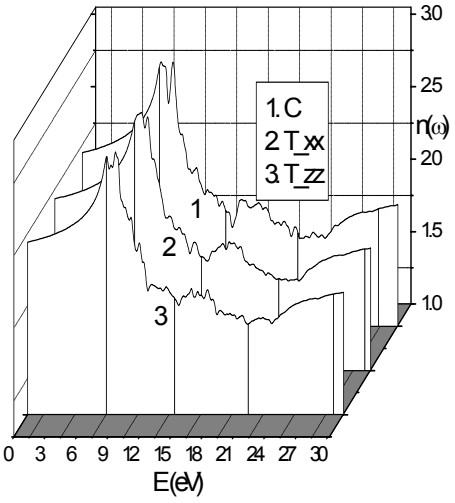

Fig. 9. The refractive index of $KNbO_3$.

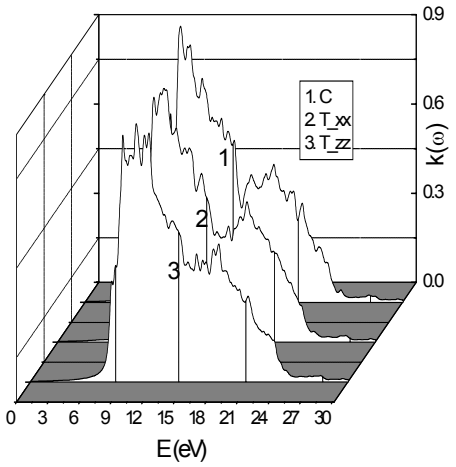

Fig. 10. The extinction coefficient of $KNbO_3$.

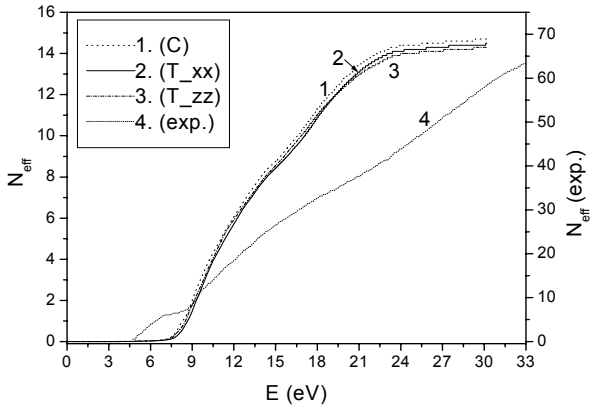

Fig. 11. The calculated effective number of electrons (N_{eff}) per unit cell of $KNbO_3$.

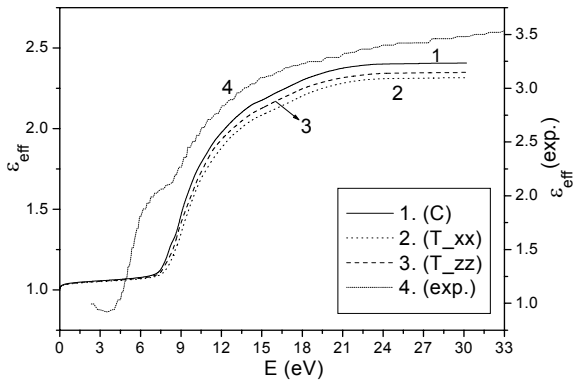

Fig. 12. The calculated effective optical dielectric constant (ε_{eff}) per unit cell of $KNbO_3$.

References

[1] M. E. Lines, A. Glass, Principles and Applications of Ferroelectric and Related Materials, Oxford Clarendon Press, (1977).

[2] A. Shigemi, T. Wada, Mat. Res. Soc. Proc. **902E,** 0902-T10-46.1 (2006).

[3] K. Kuepper, A. V. Postnikov, A. Moewes, B. Schneider, M. Matteucci, H. Hesse, M. Neumann, J. Phys: Condens. Matter **16**, 8213 (2004).

[4] E. Mamonotov, T. Egami, W. Dmowski, T. Dog, C. Venkataraman, Phys. Rev.B **66,** 224105 (2002).

[5] S. Saha, T. P. Sinha, Phys. Rev. B **62,** 8828 (2000).

[6] S. H. Wemple, M. Jr. DiDomenico, Phys. Rev. B **3,** 1338 (1971).

[7] B. T. Matthais, Phys. Rev. **75,** 1771(1949).

[8] M. Adachi, Y. Akishige, T. Asahi, K. Deguchi, K. Gesi, K. Hasebe, T. Hikita, T. Ikade, Y. Iwata, Landolt-Börnstein: Group III Condensed Matter, Oxide, subvolume A. (2002).

[9] R. Cohen, H. Krakauer, Phys. Rev. B **42,** 64 (1990).

[10] A. V. Postnikov, T. Neumann, G. Borstel, M. Methfessel, Phys. Rev. B **48,** 5910 (1993).

[11] A. V. Postnikov, T. Neumann, and G. Borstel, Phys. Rev.B **50,** 758 (1994).

[12] O. K. Andersen, Phys. Rev. B **12,** 3060 (1975).

[13] R. D. King-Smith, D. Vanderbilt, Phys. Rev. B **49,** 5828 (1994).

[14] W. Zhong, R. D. King-Smith, D. Vanderbilt, Phys. Rev. Lett. **72,** 3618 (1994).

[15] D. J. Singh, L. L. Bouer, Ferroelectrics **136,** 95 (1992).

[16] R. Yu, H. Krakauer, Phys. Rev. Lett. **74,** 4067 (1995).

[17] D. J. Singh, Ferroelectrics **164,** 143 (1995).

[18] T. Neumann, G. Borstel, Scharfschwerdt, M. Neumann, Phys. Rev. B. **46,** 10623 (1992).

[19] R. D. King-Smith, D. Vanderbilt, Ferroelectrics **136,** 85 (1992).

[20] R. Resta, M. Posternak, A. Balderechi, Phys. Rev. Lett. **70,** 1010(1993).

[21] A. M. Mamedov, L. S. Gadzhieva, Sov. Phys. Solid State **26 (9)**, 1732 (1984).

[22] E. E. Krasovskii, O. V. Krasovska, W. Schattke, J. Electron Spectrosc. Relat. Phenom **83**, 12 (1997).

[23] C-G. Duan, W. N. Mei, J. Lui, J. R. Handy, J. Phys: Condens. Mater **13**, 8181 (2001).

[24] P. Pertosa, F. M. Michel-Calendini, Phys. Rev. B **17**, 2011 (1978).

[25] C. M. I. Okoye, J. Phys: Condens. Matter **15**, 5945 (2003).

[26] N. Troullier, J. L. Martins, Phys. Rev. B **43,** 1993 (1990).

[27] M. Fuch, Scheffler, Comput. Phys. Commun. **119,** 67 (1999).

[28] W. Kohn, L. J. Sham, Phys. Rev. **140,** A1133 (1965).

[29] M. C. Payne, M. P. Teter, D. C. Allan, T. A. Arias, J. D. Joannopoulos, Reviews of Modern Phys. **64,** 1045 (1992).

[30] X. Gonze, J-M. Beuken, R. Caracas, F. Detraux, M. Fuchs, G-M. Rignanes, F. Jollet, M. Torrent, A. Roy, M. Mikami, Ph. Ghosez, J-Y Raty, D. C. Alan, Comp. Mater. Sci. **25,** 478 (2002).

[31] http:// www.abinit.org

[32] J. P. Perdew, Y. Wang, Phys. Rev. B **45,** 13244

(1992).
[33] D. M. Ceperley, B. J. Alder, Phys. Rev. Lett. **45,** 566 (1980).
[34] G. Lehman, M. Taut, Phys. Stat. Sol.(b) **54,** 469 (1972).
[35] A. W. Hewat, J. Phy. C **6**, 1074 (1973).
[36] H. J. Monkhorst, J. D. Pack, Phys. Rev. B **140,** A1333 (1976).
[37] O. Dieguez, K. M. Rabe, D. Vanderbilt, Phys. Rev. B **72**, 144101 (2005).
[38] A. Shigemi, T. Wada, Jpn. J. Appl. Phys., **44**, No.**11**, 8048 (2005).
[39] Z. Wu, R. E. Cohen, D. J. Singh, Phys. Rev. B **70**, 104112 (2004).
[40] E. Wiesendanger, Ferroelectrics **6**, 263 (1974).
[41] F. M. Michel-Calendiri, H. Chermette, J. Phys. C: Solid State Phys. **14**, 1179 (1981).
[42] F. M. Michel-Calendiri, G. Meslard, J. Phys. C **6**, 1709 (1973).
[43] M. Fox, Optical Properties of Solids, Oxford University Press, USA, (2002).
[44] D. Pines, Elementary Exications in Solids, NY-Amsterdam Benjamin Inc. (1963).
[45] B. Hammer, L. B. Hansen, J. K. Norskov, Phys. Rev. B **59**, 7413 (1999).
[46] W. Kleemann, F. J. Schafer, M. D. Fontana, Phys. Rev. B **3**, 1148 (1984).

*Corresponding author: scabuk@cu.edu.tr